Comparison of Classical and Modern Missile Autopilot Design and Analysis Techniques

A. Arrow*
Johns Hopkins University, Laurel, Maryland
and
D. E. Williams†
The Singer Company, Little Falls, New Jersey

A subject of considerable debate for several years has been the merits of modern control system design and analysis techniques compared to the more classical techniques of Bode and Nyquist. This paper documents a case study comparing these techniques as applied to an advanced air-to-air interceptor being considered by the U.S. Air Force as part of the Extended Medium Range Air-to-Air Technology program. The specific modern design technique is the linear quadratic Gaussian technique with loop transfer recovery. Both designs are initiated with the same set of requirements for the same vehicle. The comparison considers not only robustness of design but also the complexity of implementing the two designs and the analysis required to validate each design.

Nomenclature

A,B,C,D	= modern control law matrices
$K_1,K_2,\ldots,K_{11}$	= classical control law gains
$K(s),L(s),P(s)$	= compensator, perturbation, plant matrices
p,q,r	= missile angular velocities about body-fixed axes $\bar{x}_B,\bar{y}_B,\bar{z}_B$
P,R	= constant or equilibrium roll and yaw rate
$Q,\bar{Q}$	= dynamic pressure, estimated Q
r_c	= commanded yaw angular rate about $\bar{z}_B$
u_q,u_r,u_p	= commanded pitch, yaw, roll control incidence for no aerodynamic control cross-coupling
$\bar{V}$	= estimated missile velocity
$\bar{x}_B,\bar{y}_B,\bar{z}_B$	= body-fixed roll axis positive forward, pitch axis positive starboard, yaw axis
$\alpha,\bar{\alpha}$	= angle-of-attack, estimated α
$\beta,\bar{\beta}$	= sideslip angle, estimated β
$\delta_{p_c},\delta_{Q_c},\delta_{R_c}$	= commanded roll, pitch, yaw control incidence
$\eta_{Q_c},\eta_{y_c},\eta_{z_c}$	= commanded acceleration in $-\bar{z}_B$, $\bar{y}_B$, and $\bar{z}_B$ direction
η_Q,η_R	= achieved pitch and yaw normal accelerations in $-\bar{z}_B$ and $\bar{y}_B$ directions
ϕ	= roll angle = $\int p\,dt$
ϕ_e	= roll angle error

I. Introduction

STATE space methods for the design of autopilots for tactical missiles have received considerable attention in the literature but few practical applications. It is well known that these methods are well suited to highly coupled, multiple-input-multiple-output dynamic processes characteristic of high-performance interceptors, but no direct comparison has been made of the performance of autopilots designed using state-space methods with autopilots designed by more conventional, frequency-domain methods.

The goal of this study is a quantitative comparison of two autopilot designs for the same high-performance advanced tactical missile. One design is obtained using the linear quadratic Gaussian loop transfer recovery (LQG/LTR)[1] technique of state-space design methodology. The other design is based on use of conventional design methods validated by experience as appropriate for this type of missile.[2,8] The Extended Medium Range Air-to-Air Technology (EMRAAT) missile was selected for this study; dynamic characteristics were furnished by the Air Force Armament Laboratory (AFATL). This missile is an extended medium-range air-to-air high-performance missile, which achieves its maneuvering capability by banking to turn (BTT).

The purpose of the autopilot is to control the EMRAAT missile during rapid roll rates and large maneuvers, without exceeding stated requirements, at a high- and a medium-altitude flight condition. This was an ambitious undertaking because BTT missile autopilot designs that are mature (i.e., include actuator dynamics and nonlinearities, elastic body modes, and nonlinear cross-coupled aerodynamics) have not been able to produce levels of response typical of skid-to-turn (STT) controlled missiles.[4] Moreover, there have been concerns as to whether tactical speeds of response during the terminal phase can be achieved owing to kinematic and inertial coupling. These couplings increase in severity with more rapid roll rates and increasing airframe asymmetry (the EMRAAT missile is asymmetrical).[4]

The study that was performed includes a linear analysis of both autopilot designs from classical and modern viewpoints and a 6-degree-of-freedom (DOF) simulation using the nonlinear aerodynamic model provided by AFATL.

II. Design Goals and Requirements

The function of any missile autopilot is threefold: 1) maintain stability of the airframe over the performance envelope, 2) provide adequate airframe response for the guidance system, and 3) reduce sensitivity of guidance performance to vehicle parameter variations and disturbances. The degree to which these functions must be performed is determined by system characteristics such as targets, airframe parameters, guidance system, and warhead lethality.

Received Aug. 5, 1987; presented as Paper 87-2581 at the AIAA Guidance, Navigation and Control Conference, Monterey, CA, Aug. 17-19, 1987; revision received Nov. 9, 1987.

*Senior Engineer, Applied Physics Laboratory. Member AIAA.
†Staff Member, Kearfott Guidance Navigation Division.

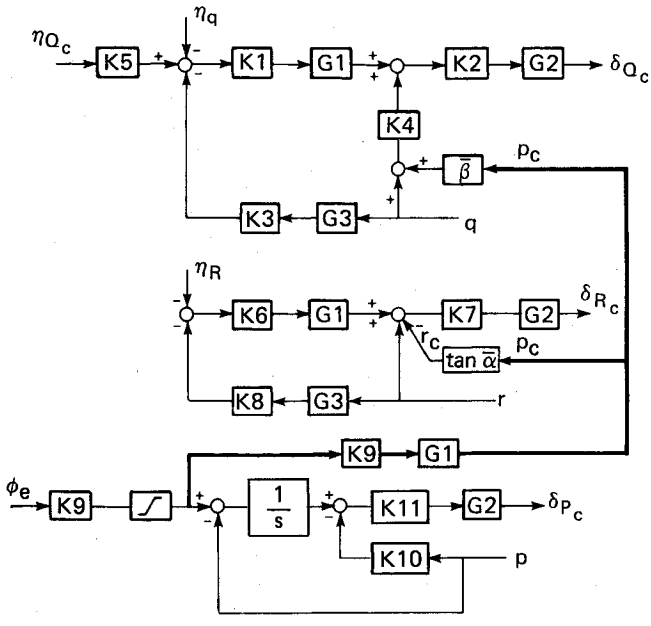

G1 = 1/(0.1 s + 1) G2 = (s/12 +1)/s G3 = s/(s/200 + 1)

Fig. 1 Classical control law.

In order to quantify the functions of a missile autopilot for comparison or design purposes, a set of measures has been developed for iterative classical design procedures. Modern autopilot design procedures have not yet established such a quantified set of measures. Therefore, for comparison purposes, this study uses the same set of requirements for both design techniques.

Following is a list of autopilot design requirements for EMRAAT:

1) Preferred maneuver plane acceleration time-constant goals: 0.3 s at 40K ft, $M = 2.5$, empty; 0.5 s at 65K ft, $M = 3.0$, empty.

2) Compensation for elastic body modes: attenuation in actuator command branch pitch, yaw -15 dB at 100 rad/s, 1st mode at 234.2 rad/s (37.3 Hz); roll -0 dB at 100 rad/s, 1st mode estimate 90 Hz.

3) Actuator constraints: 30 Hz, first order or 45 Hz, 0.7 damping ratio, second order; 300 deg/s, 55 deg.

Preferred maneuver plane acceleration time-constant goals are specified for the two flight conditions investigated. The time constant, as defined for this study, is the time for the response due to a step function command to reach 63% of the final value. The time constants are consistent with the size of the EMRAAT missile.

Adequate loop attenuation of measured missile bending frequencies must be achieved or reinforcement of bending motion will occur. This, in turn, could lead to loss of control effectiveness due to actuator saturation and instrument isolation problems. High-frequency notch filters are used to attenuate critical modes and, because of model uncertainty, a finite width to these notches has to be maintained that, in turn, introduces phase lag at lower frequencies with associated stability problems. Tactical speeds of response, requiring wider control bandwidth, compound this problem. The problem is alleviated by using low-frequency dynamic compensators to provide extra-high-frequency attenuation. Classical design experience has shown that the low-frequency autopilot design should be able to provide the attenuation requirements listed. This will help high-frequency notch filter design to satisfy the overall elastic attenuation requirement.

The actuators of the actual EMRAAT missile have yet to be specified. For purposes of autopilot design, a first-order model with a 30-Hz bandwidth was assumed for the classical design approach. The design software that implements the state-space approach is based on a second-order actuator model; hence, a second-order model with a natural frequency of 45 Hz with a damping ratio of 0.7 was assumed. The two models are close in gain and phase out to frequencies of 100 rad/s. After 100 rad/s, the second order has more attenuation. In performance simulations, the actuators are constrained to limits of 300 deg/s and 55 deg.

III. Linear Analysis of Autopilot Designs

A linearized dynamic airframe model was developed for stability analyses of both autopilots in the frequency domain. Airframe dynamics are linearized at fixed flight conditions (i.e., constant velocity, altitude, and mass parameters) and by constraining the missile to particular maneuvers. Fixed flight conditions and maneuvers with constant angles of attack result in a linear model of the form that has been useful for design and analysis of STT-controlled vehicles. This model is expanded to include one type of coordinated motion (i.e., minimum sideslip)[4] for BTT control. The missile rolls about its velocity vector with constant angle of attack α_e and constant values of roll rate P_e and yaw rate R_e, where $R_e = P_e \tan\alpha_e$ and subscripts e denote equilibrium values. It must be noted, however, that the motion of the EMRAAT missile, due to step function acceleration commands or the selected guidance scenarios on a 6-DOF simulation, does not exhibit a constant roll rate. As a result, the linearization is not strictly valid. The resulting linear airframe model has merit as a design tool only if the resulting control law satisfies the functions of a missile autopilot.

The classical CBTT (coordinated BTT) control law for EMRAAT[8] is shown in Fig. 1. Measurements of missile body angular rates (p,q,r) and normal accelerations (η_Q,η_R) are used to determine actuator commands ($\delta_{Q_c},\delta_{R_c},\delta_{P_c}$). The autopilot cross-coupling branches shown in bold lines provide coordinated motion between roll and yaw channels and reduce the effect of kinematic coupling into the pitch channel.[2,8] For the linear airframe dynamics model, the coordinating command r_c is equal to $p_c\alpha_e + \alpha P_e$. The autopilot is commanded by pitch acceleration command η_{Q_c}, and roll angle error ϕ_e. For linear studies, ϕ_e is approximated by $-\phi$, where roll angle $\phi = \int p\, dt$.

The linearized modern CBTT control law is shown in Fig. 2. The gain matrices for one of the flight conditions are given in Appendix A. The autopilot is commanded by pitch acceleration command η_{Z_c} (i.e., $-\eta_{Q_c}$) and the negative of roll angle error ϕ_e. The decoupling transformation is used to decouple the aerodynamic control cross coupling of the yaw and roll channels. The modern control law has 51 gains, which may be functions of $p, p^2, \bar{Q}, \bar{Q}^2, \bar{V}, \bar{V}^2$, and $\bar{V}^3$. In its present form, the control law is more complex to implement than the classical control law, which has 11 gains that are functions of $\bar{Q}$, $\bar{Q}^{1/2}$, $\bar{\beta}$, $\bar{\alpha}$, and $\bar{V}$. Both control laws are eighth order and require estimation (denoted by the bar) of dynamic pressure $\bar{Q}$ and velocity $\bar{V}$. The classical control law requires, in addition, estimates of the sideslip angle $\bar{\beta}$ and angle of attack $\bar{\alpha}$. The modern design requires an estimate of angle of attack for the purpose of decoupling the control variables of the pitch/yaw channel from the roll channel.

A comparison of the autopilot design approaches is summarized in Table 1. The decoupling approach used in the modern design could also be used in the classical design, if necessary, for further improvement of relative stability at high angles of attack. However, as currently configured, there are major differences in the two approaches for achieving robustness, responsiveness, and coordination of maneuvers.

Relative stability was determined classically (i.e., one branch at a time) for all branches of the classical autopilot. For the modern autopilot, classical margins were determined at each measurement, actuator command, and branch of the decoupling transformation. Multiloop robustness of the autopilots was evaluated from the singular value decomposition of an

Table 1 Autopilot design approach

Property	LQG/LTR	Classical
High angle-of-attack stability	Direct nulling approach to decoupling lateral channel	Indirect approach to decoupling using wide-bandwidth rate loops
Robustness	Unstable wide bandwidth pitch rate loop and very wide bandwidth acceleration loop	Stable, wide bandwidth rate loops with integrators
Rapid response	Very wide bandwidth pitch acceleration loop	Angular acceleration feedback, wide bandwidth rate loops
Coordination	Cross-coupling pitch and yaw channels via roll rate	Autopilot cross coupling from commanded roll rate to yaw channel

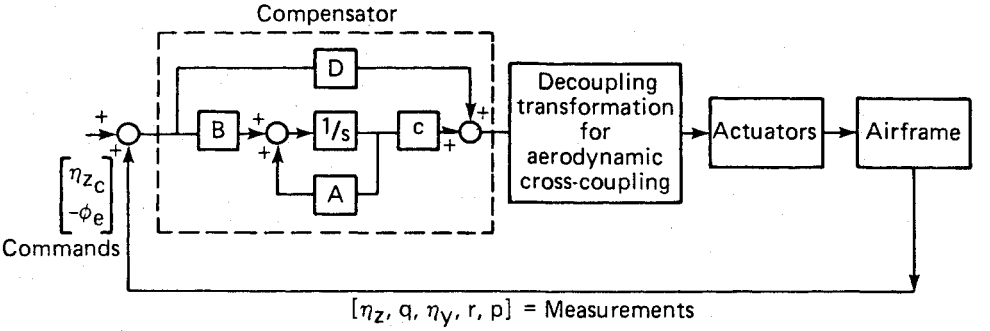

Fig. 2. Linear model of modern autopilot.

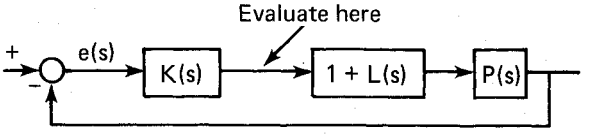

Fig. 3 Robustness evaluation.

appropriate return difference matrix over the frequency range of interest.

Since classical gain and phase margins are based on multiplicative gain and phase margins, respectively, a similar type of error structure is assumed for the multiloop situation considered here. Specifically, the perturbation element used is of the form $I + L(s)$, shown in Fig. 3, where robustness for both autopilot designs is evaluated at the actuator inputs only. The reason it cannot be evaluated at the outputs is that there are more measurements than inputs and the required inverse of the loop transmission matrix does not exist. The multiloop gain margin and phase margins[6] are evaluated as follows:

$$\text{Gain margin} = 1 - \mu \text{ to } 1 + \mu,$$

$$\text{Phase margin} = \pm 2 \sin^{-1}(\mu/2) \tag{1}$$

where $\mu = \underline{\sigma}[I + G^{-1}(s)]$ *for* $s = j\omega$, $\underline{\sigma}[I + G^{-1}(s)]$ is the minimum singular value of $I + G^{-1}(s)$, where $G(s)$ is the nominal loop transmission corresponding to the break point at which the perturbation is assumed to be present.

To interpret the gain and phase margin results, assume that the perturbation matrix $L(s)$ is diagonal. If all of the elements of $L(s)$ are real (pure gain changes), then simultaneously all of the elements of $L(s)$ can vary between $\pm\mu$, and the perturbed closed-loop system will remain stable. Similarly, if all of the diagonal elements of $L(s)$ can vary between $e^{\pm j\theta}$ and then the perturbed closed-loop system is guaranteed to be stable.

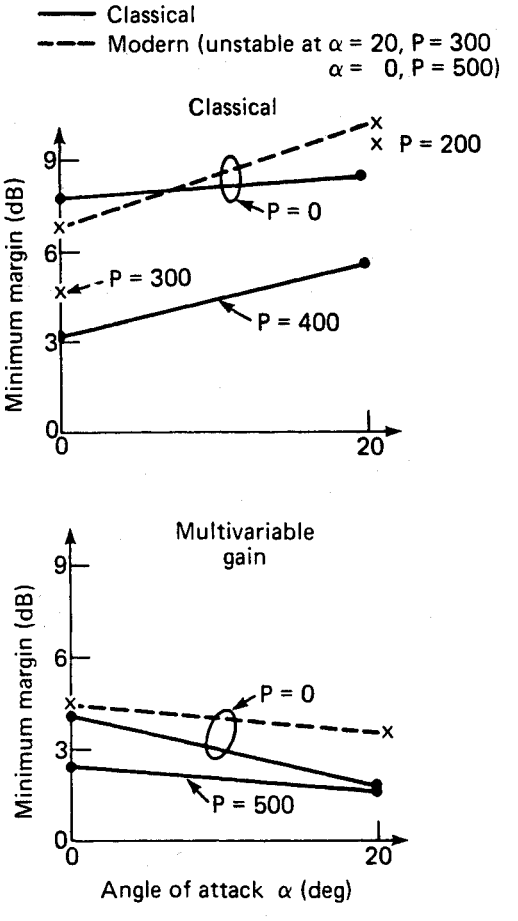

Fig. 4 Comparison of gain margins at 65,000-ft altitude.

A comparison of classical and multivariable margins for both autopilots is shown in Figs. 4–7. Minimum classical margins are shown, with no distinction as to whether they are increasing or decreasing margins or as to the branch in which they occur. Increasing/decreasing margin refers to whether the gain or phase may be increased/decreased before instability occurs. Minimum multivariable gain margins are all increasing margins. Robustness increases for multivariable margins as the gain increases. Twenty degrees angle of attack is the extremity of available EMRAAT aerodynamics. For the 65,000-ft altitude condition, the classical autopilot limits the commanded roll rate to 300 deg/s. This limit was used because it was sufficient to satisfy required response times, and also 6-DOF studies showed that high roll rates would result in stability problems due to actuator limiting. For both flight conditions, the classical autopilot is stable over required angles of attack and roll rates. Increasing roll rate is destabilizing for the multivariable margins of both autopilots. However, for classical margins, increasing roll rate is destabilizing at 65,000 ft and stabilizing at 40,000 ft for the classical autopilot. For both altitudes, increasing roll rate is destabilizing for the classical margins of the modern autopilot, and instability is predicted for a combination of high angles of attack and high roll rates. The instability is due to the approximation used in the design of the pitch/yaw observer, where filter gains (which, using the design procedure, would be a function of roll rate and/or dynamic pressure) were approximated as constants. No actual instability has been encountered, however, in 6-DOF simulation studies. Moreover, since the combination of high roll rate and high angles of attack is highly unlikely because of the command logic for the modern autopilot, it is not regarded as a serious problem.

The multivariable results demonstrate that the modern autopilot is more robust for $P = 0$ and for perturbations reflected to the airframe inputs. Robustness for both autopilots decreases with increasing angles of attack, but the modern design maintains greater robustness. The conservatism of the increasing multivariable gain margin was checked for the classical autopilot at 40,000 ft, $\alpha = 20$, $P = 0$. Although the indicated margin is only 2.1 dB, all gains in the actuator command branches were increased as much as 6 dB with no stability problem. In addition, since the majority of minimum classical margins do not occur for actuator command branches, the critical multivariable margins may not be at the inputs to the airframe.

For $P = 0$, the classical margins of the modern autopilot are greater than the desired 6 dB and 30 deg for both altitudes. The classical autopilot has desirable classical margins at 65,000 ft. At 40,000 ft, however, the gain reduction margin for the yaw gyro decreased to 3.9 dB. This is probably acceptable (i.e., ≥ 3 dB) because it occurs at maximum α and, therefore, would occur for a short time interval during a maneuver. It could be improved by adding controls decoupling as used in the modern autopilot.

Sensitivity of the autopilots to uncertainties in the most critical aerodynamic stability derivatives is shown by the classical, one branch at a time, gain margins in Table 2. Both autopilots exhibit robustness due to aerodynamic cross coupling (i.e., a minimum of 6 dB is desired).

To maintain stability due to missile body elastic modes, a requirement of -15 dB at 100 rad/s was specified. The attenuation of the open pitch actuator command is compared for the two designs in Fig. 8. The attenuation of the modern autopilot is less than 15 dB at 100 rad/s but close enough for acceptance. However, in this design, the gain does not roll off until 300 rad/s.

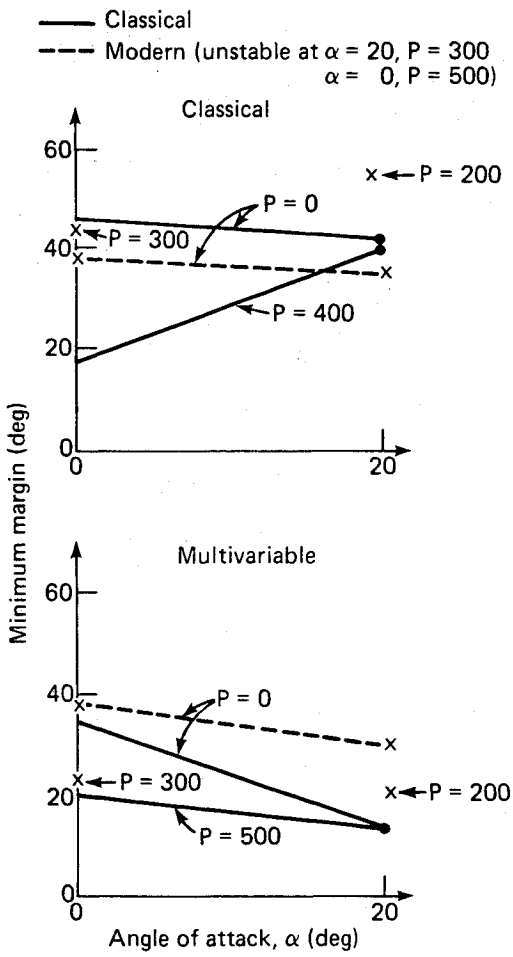

Fig. 5 Comparison of phase margins at 65,000-ft altitude.

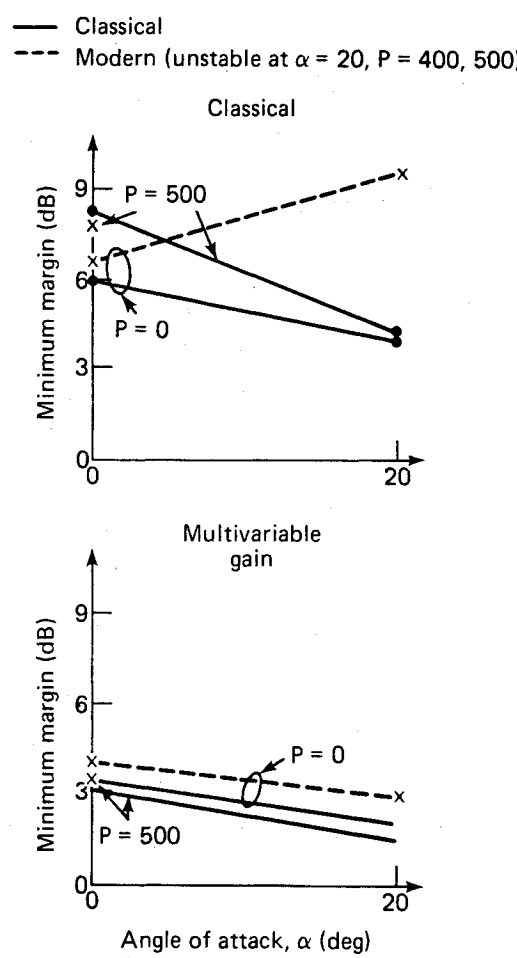

Fig. 6 Comparison of gain margins at 40,000-ft altitude.

The same situation exists for the open yaw actuator command of the modern autopilot, although the open roll actuator command of the modern autopilot satisfies the attenuation requirement of zero dB or more at 100 rad/s and provides more attenuation than the open classical autopilot actuator commands at 65,000 ft. The attenuating properties for the three actuator commands at 40,000 ft are the same as at 65,000 ft. The reason for the higher gain of the modern system over elastic frequencies is due to the accelerometer path shown in Fig. 9. The gyro branch of the modern system has the same attenuation as the classical system, which was considered to have a wide bandwidth.

Sensitivity of the autopilots to guidance or pitch accelerometer noise is shown in Fig. 10. The gain is from η_Q to δ_{Q_c} in Fig. 1 (gain is 1.2 dB more from η_{Q_c} to δ_{Q_c}) for the closed-loop classical autopilot. The gain is η_z or η_{z_c} to pitch actuator command, shown in Fig. 2 for the closed-loop modern autopilot. The modern autopilot has significantly more gain than the classical autopilot at high frequencies. This could result in actuator saturation and control problems.

Although the attenuation from accelerometer to actuator command was not specified as a design requirement, its effect should be considered. Sensitivity of the autopilots due to pitch gyro noise is shown in Fig. 11. The gain is shown from an input into the pitch gyro (q, in Figs. 1 and 2) to the actuator command δ_{Q_c} for the closed-loop autopilots. The gain of the modern system is considerably larger at high frequencies compared to the classical autopilot. This again could result in actuator saturation and control problems.

The same sensitivities shown in Figs. 10 and 11 for the pitch channel of the modern autopilot also occur in the yaw channel. A comparison of the sensitivity due to roll gyro noise (i.e., gain from an input into the roll gyro p in Figs. 1 and 2 to δ_{p_c} or roll actuator command) is the same for both autopilots. The

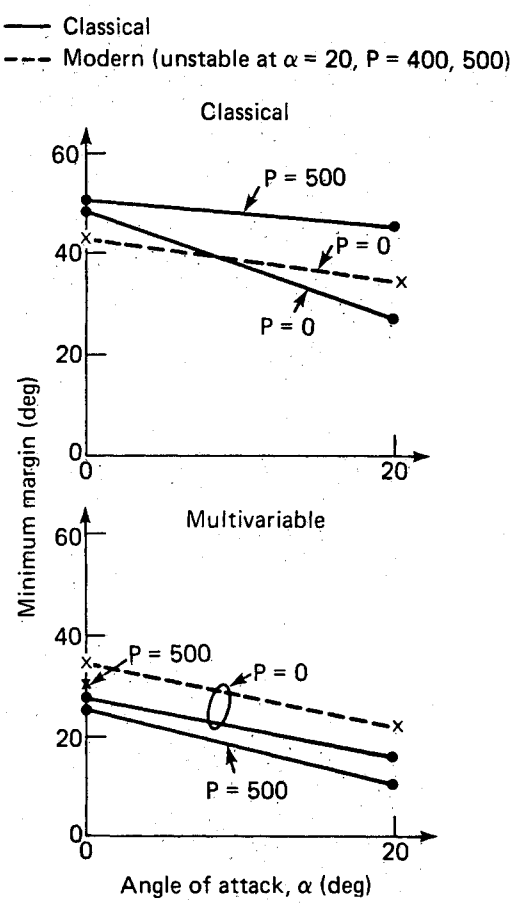

Fig. 7 Comparison of phase margins at 40,000-ft altitude.

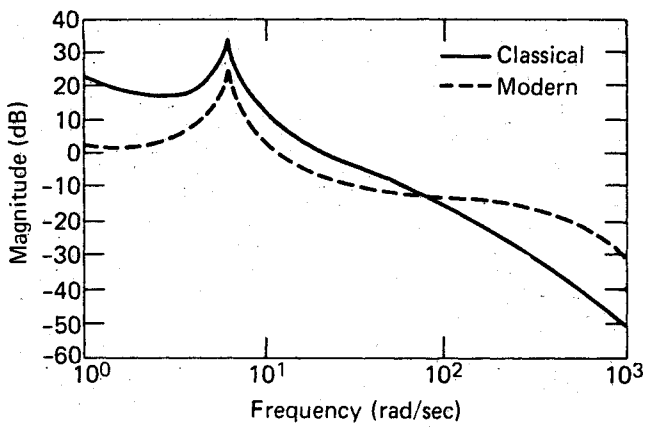

Fig. 8 Attenuation at open pitch actuator command (65,000 ft, $\alpha = 0$, $P = 0$).

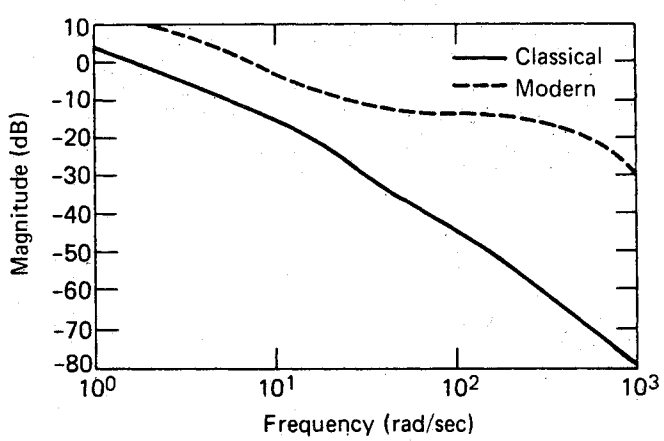

Fig. 9 Attenuation at open pitch accelerometer output (65,000 ft, $\alpha = 0$, $P = 0$).

Table 2 Aerodynamic cross-coupling sensitivity

	Classical				LQG/LTR ($P = 0$)			
	40,000 ft		65,000 ft		40,000 ft		65,000 ft	
Cross coupling	$P = 0$	$P = 500$	$P = 0$	$P = 400$	$P = 0$	$P = 300$	$P = 0$	$P = 200$
$C_{\ell_{\delta R}}$	20.2	19.9	17.9	17.7	8.2	8.0	19.2	18.6
$C_{n_{\delta P}}$	15.5	15.5	13.9	7.0	32.2	31.9	39.7	39.7
C_{ℓ_β}	13.5	16.4	11.6	11.4	45.0	41.5	49.6	49.6

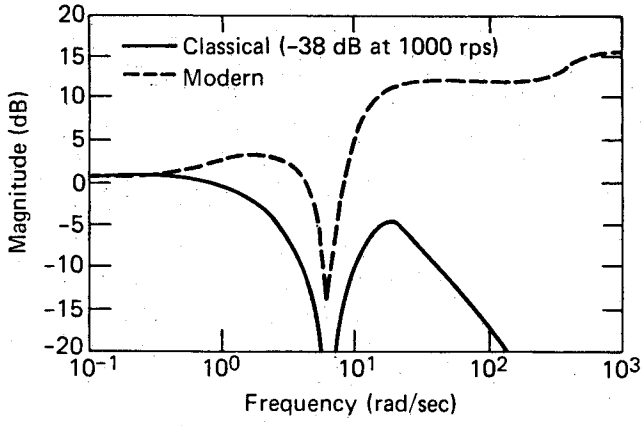

Fig. 10 Pitch acceleration command or accelerometer output to pitch actuator command (65,000 ft, $\alpha = 0$, $P = 0$).

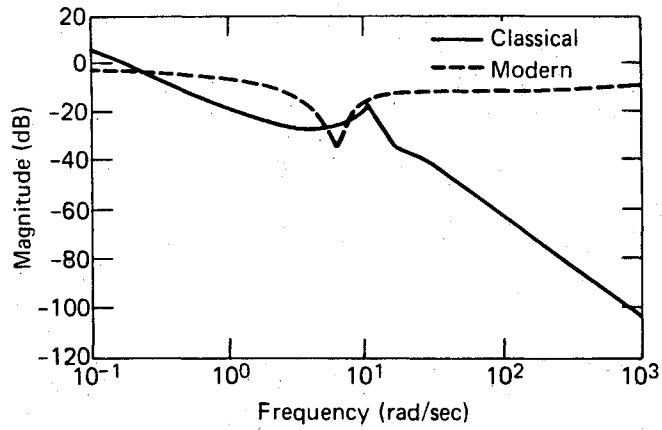

Fig. 11 Pitch gyro output to pitch actuator command of closed-loop autopilots (65,000 ft, $\alpha = 0$, $P = 0$).

Table 3 Summary of desired maneuver plane time constants, s

	40,000 ft, Mach 2.5				65,000 ft, Mach 3.0	
	15 gees (0, 180 deg)		15 gees (90, 270 deg)		9 gees (0, 180 deg)	
	0 deg	180 deg	90 deg	270 deg	0 deg	180 deg
Classical	0.2	0.3	0.25	0.31	0.44	0.4
Modern	0.1	0.49	0.17	0.44	0.2	0.5

sensitivity of guidance noise to the roll actuator is shown in Fig. 12. The gain is shown from a commanded roll angle ϕ_c (which is not shown in Figs. 2 and 3 but is calculated by using $\phi_e = \phi_c - \phi$ where $\phi = \int p\, dt$). The high-frequency gain of the modern autopilot is significantly higher than the classical design.

IV. Nonlinear Analysis of Classical and Modern Autopilots

The command logic used by the autopilots for positive angle-of-attack BTT control are different. The classical autopilot applies the total magnitude of guidance acceleration command in the preferred maneuver or positive angle-of-attack direction. The modern autopilot resolves the guidance command onto the preferred maneuver axis and, if it goes in the negative angle-of- attack direction, the command is opened. The roll angle error for both autopilots is calculated from body-fixed guidance acceleration commands (η_{y_c} = yaw, η_{z_c} = pitch), where $\phi_e = \tan^{-1}(\eta_{y_c}/-\eta_{z_c})$ for the classical and $-\phi_e$ for the modern.

Acceleration responses[3] in the desired maneuver plane due to a series of step function acceleration commands were performed on a 6-DOF simulation. During the first 1-s time interval, antigravity bias is applied and initial conditions established. A 15-gee command is applied during the second 1-s time interval in the upward (0-deg) preferred maneuver direction so that the missile is not forced to roll and maneuvers like a STT-controlled missile. During the third 1-s time interval, the missile is forced to roll 180 deg to maintain positive angles of attack as a 15-gee command is applied in the downward direction (180 deg). The response of the modern autopilot is much faster than the classical autopilot or design goals, as predicted in linear studies, except for 180-deg roll maneuvers. The delay in the response is caused by a slow roll response (i.e., 0.4-s time constant, 430-deg/s maximum roll rate). The same delay results for a series of commands in the 90-deg, or starboard, and 270-deg, or port, directions when the missile is forced to roll 180 deg (i.e., roll angle time constant is 0.38 s, maximum roll rate 430 deg/s). The delay results in time constants that are larger than desired at 40,000 ft but not at 65,000 ft, as shown in Table 3. The classical autopilot response is either faster than, or meets, design goals.

Classical and modern autopilots were compared during terminal homing engagements against a constant-speed maneuvering target. The scenarios are shown in Figs. 13 and 14, where crossing angle is the parameter. The target is modeled as a point mass capable of instant acceleration changes normal to the velocity vector. One step of acceleration occurs at 6000-ft range and another at 1-s time-to-go. Target maneuver directions are normal to target velocity and have a component normal to the encounter plane. The guidance law is designed using optimal control theory[7] and requires estimates of relative position and velocity and time-to-go. It is assumed that the commanded acceleration is derived on the basis of error-free knowledge of the motion (position, velocity, and acceleration) of the interceptor and the target. Autopilot instrumentation (gyro and accelerometer) errors are representative of state-of-the-art instruments. Acceleration commands to the autopilot are limited to keep angles of attack less than 20 deg.

A performance comparison of the two autopilots based on final miss distance is shown in Table 4. In most simulated engagements, but not all, the modern autopilot design achieves lower terminal miss distances. It also exhibits faster response to guidance commands than the classical autopilot.[3] This faster response, which may be attributed to the wider bandwidth of the modern design, is accompanied by control saturation at 40,000 but not at 65,000 ft. Both autopilots keep sideslip to within 5 deg. However, sideslip angle for the modern autopilot is smaller and better damped. Additional studies are needed to investigate impact of final engagement geometry on miss distance for BTT-controlled missiles. Small variations in commanded acceleration levels can result in large changes in terminal banking maneuvers and miss distance.

Table 4 Miss distances

	Crossing angle, deg	Modern, ft	Classical, ft
40,000	10	10.5	24.4
	15	30.0	29.5
	20	[a]	36.5
	25	41.7	47.6
	30	33.6	[a]
	40	[a]	[a]
65,000	5	13.4	28.6
	7	15.4	42.8
	10	18.3	42.8
	12	[a]	17.4
	15	[a]	[a]

[a]Miss distance > 50 ft.

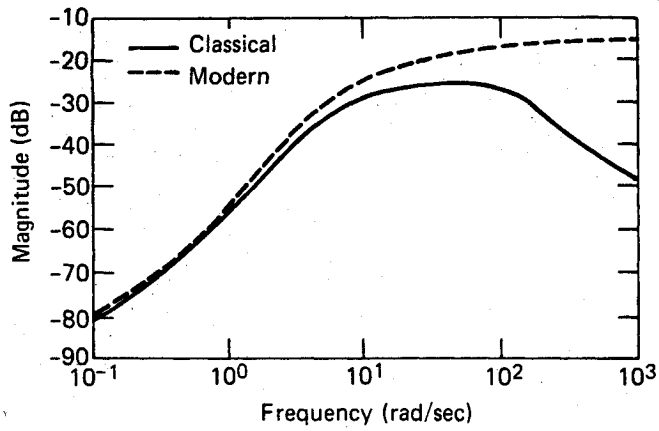

Fig. 12 Roll angle command to roll actuator command of closed-loop autopilots (65,000 ft, $\alpha = 0$, $P = 0$).

40K: Initial range : 15,000 ft
Missile velocity : 2419 ft/sec (M = 2.5)
Target velocity : 1938 ft/sec (M = 2.0)
Target acceleration : 9g

65K: Initial range : 15,000 ft
Missile velocity : 2903 ft/sec (M = 3.0)
Target velocity : 2227 ft/sec (M = 2.3)
Target acceleration : 3g

Fig. 13 Scenarios.

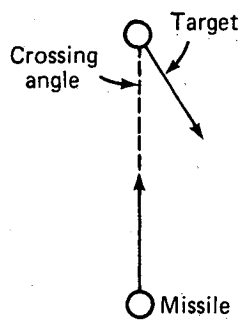

Fig. 14 Missile-target geometry.

V. Adaptability to Development

The modern and classical BTT missile autopilot designs compared in this study have both progressed to the level at which engineering development guidance and autopilot studies are required to evaluate whether they can be implemented. Engineering development level simulations include the extra detail that can be obtained only when detailed hardware constraints are considered.

Detailed hardware specifications are not available for the EMRAAT airframe considered in this paper. However, classical design experience has shown that preliminary predictions are very optimistic compared to the performance actually achieved by hardware. With this in mind, the following topics are considered:

1) High-frequency attenuation: The higher gain of the modern system may complicate the high-frequency filter design in order to satisfy the overall elastic attenuation requirement. This could, in turn, require modifications in the low-frequency autopilot design.

2) Noise sensitivity: Larger high-frequency gain of the modern design may result in actuator saturation and control problems in response to guidance noise.

3) Radome errors: Sensitivity of the autopilot designs to radome boresight errors[5] has not been evaluated.

The first two topics may be addressed if necessary in the modern design by changing weightings of the full-state feedback design and reduced-order observer or by using a full-state observer, filtering the guidance commands, or both. Toward this end, the autopilot design requirements listed in Sec. II should be expanded for the modern design to include high-frequency roll-off (i.e., attenuation per decade) and attenuation at a number of frequencies for actuator input and noise rejection frequency responses. Because of the nonsquare nature of the system (more outputs than inputs), the modern design technique has applied the LQG/LTR procedure only at the input to the plant. This does not guarantee the required noise rejection represented by the high-frequency attenuations of the responses in Figs. 9–11. In addition, increasing high-frequency attenuation may slow down acceleration response to guidance commands which may, in turn, increase miss distances. Further work is needed to develop practical multivariable loop-shaping techniques that can be applied to the input or output of a general nonsquare plant.

To address some of the potential shortcomings of the modern design, a preliminary redesign study[1] of the pitch/yaw autopilot was undertaken after the comparative analysis of this paper was completed. Weightings were changed in the full-state feedback design and for the reduced-order observer. This resulted in the same high-frequency attenuation at the actuator inputs as the classical design, a slight improvement in multivariable margins, and elimination of control saturation. Although these improvements were achieved at the expense of a slower acceleration response, miss distance of the 40,000-ft/25-deg case in Table 4 decreased 3 ft. Turn coordination is still excellent. A follow-on study is recommended that would complete the comparison of the classical and redesigned modern autopilots by comparing noise rejection (Figs. 9–11), acceleration responses (Table 3), and a series of guided runs (Table 4) with realistic dynamics included in the target model.

The last topic, radome errors, could be addressed by both designs with hybrid control (i.e., STT at low acceleration levels and BTT at high acceleration levels).

VI. Conclusions

Modern design techniques have made considerable progress in balancing the requirements of control and robustness to plant uncertainties. Classical design techniques have also progressed by taking advantage of the latest software improvements and modern state-space methods. Modern techniques are well suited for controlling highly coupled airframes, whereas the classical technique has difficulty finding the proper

control law for such systems. The classical technique, however, appears to better account for constraints that are not explicitly modeled. It is recommended that research be continued in both modern and classical techniques and, particularly, in the merging of the two so that design techniques that maintain the best features of both can be developed.

Appendix: Gain Matrices for Modern Design

Flight conditions

$$65{,}000 \text{ ft, Mach } 3.0,\ \alpha = 0$$
$$\beta = 0,\ P = 0, \text{ empty weight}$$
$$\dot{x} = Ax + Bu$$

where

$$x' = \eta_{z_c} - \eta_z, q, \eta_y, r, \phi_e, p$$
$$u' = u_q, u_r, u_p$$
$$A = [a_{nn}]_{9\times 9}$$

where

$a_{11} = -8.8E\text{-}5$	$a_{12} = 1$	$a_{15} = 3.8E\text{-}6$
$a_{21} = -1.3E5$	$a_{22} = -500$	$a_{25} = 7.8$
$a_{33} = -3.7E\text{-}5$	$a_{34} = 1$	$a_{36} = -1.E\text{-}7$
$a_{43} = -1.2E5$	$a_{44} = -439$	$a_{46} = 163$
$a_{51} = 3.8$	$a_{52} = -375$	$a_{55} = -1.1$
$a_{72} = 1$		
$a_{87} = -8.4E4$	$a_{88} = -395$	$a_{89} = 102$
$a_{97} = 8.2E4$	$a_{99} = -100$	

$$B = [b_{nn}]_{9\times 6}$$

where

$b_{11} = -0.21$	$b_{12} = 0.011$	$b_{21} = -164$
$b_{22} = 2.8E4$	$b_{33} = 0.21$	$b_{34} = -2.8E\text{-}7$
$b_{43} = 70.2$	$b_{44} = 1.5E4$	$b_{51} = 81$
$b_{52} = -3.2E3$	$b_{85} = 1.6E4$	$b_{86} = 1.2E4$
$b_{95} = -9.3E3$	$b_{96} = -1E4$	

$$[C] = [c_{nn}]_{3\times 9}$$

where

$c_{11} = -0.63$	$c_{12} = -7.5E\text{-}4$	$c_{15} = 9.8E\text{-}4$
$c_{23} = -0.45$	$c_{24} = -2E\text{-}4$	$c_{26} = 2E\text{-}3$
$c_{37} = -5.3E\text{-}2$	$c_{38} = 1.2E\text{-}5$	$c_{39} = 1.3E\text{-}3$

$$[D] = [d_{nn}]_{3,6}$$

where

$d_{11} = -3.2E\text{-}3$	$d_{12} = 0.36$	$d_{23} = 2E\text{-}3$
$d_{24} = 0.19$	$d_{35} = 0.2$	$d_{36} = 0.15$

Decoupling transformation$_{3\times 3}$

1,1 = 1
2,2 = 0.99
2,3 = 0.15
3,2 = −0.06
3,3 = −0.99

(Elements not listed are zero).

Acknowledgments

This work was supported by JHU/APL Stuart S. Janney Fellowship and the independent research and development program of The Singer Company.

References

[1]Williams, D. E., "A Computer-Aided Autopilot Design Procedure for a High-Performance Bank-to-Turn Controlled Tactical Missile," *Proceedings of the 1987 AIAA Guidance, Navigation and Control Conference,* AIAA, New York, 1987, pp. 1354–1359.

[2]Kovach, M. J., Stevens, T. R., and Arrow, A., "A Bank-to-Turn Autopilot Design for an Advanced Air-to-Air Interceptor," *Proceedings of the 1987 AIAA Guidance, Navigation and Control Conference,* AIAA, New York, 1987, pp. 1346–1353.

[3]Arrow, A., "Comparison of Classical and Modern Autopilot Design and Analysis Techniques for a Tactical Air-to-Air Bank-to-Turn Missile," *Proceedings of the 1987 AIAA Guidance, Navigation and Control Conference,* AIAA, New York, 1987, pp. 1360–1371.

[4]Arrow, A., "Status and Concerns for Bank-to-Turn Control of Tactical Missiles," *Journal of Guidance, Control, and Dynamics*, Vol. 8, March–April 1985, pp. 267–274.

[5]Arrow, A., "Influence of Radome-Induced Body Motion Coupling on Bank-to-Turn Controlled Terminal Homing Missiles," *Proceedings of the Workshop on Bank-to-Turn Controlled Homing Missiles*, GACIAC/IIT, Sept. 19–20, 1984, pp. 317–331.

[6]Safonov, M. G. and Athans, M., "Gain and Phase Margins for Multi-loop LQG Regulators," *IEEE Transactions of Automatic Control*, Vol. AC-22, April 1977, pp. 173–179.

[7]Williams, D. E., Friedland, B., and Madiwale, A. N., "Modern Control Theory for Design of Autopilots for Bank-to-Turn Missiles," *Journal of Guidance, Control, and Dynamics*, July–Aug. 1987.

[8]Arrow, A. and Stevens, T. R., "Preliminary Autopilot Study for the U.S. Air Force Compact Extended Medium Range Air-to-Air Technology Missile Configuration," JHU/APL Rept. FS-87-124, July 1987.